

E18-2007-111

Yu. V. Taran, A. M. Balagurov, S. G. Sheverev, J. Schreiber¹,
H. Bomas², A. M. Korsunsky³

INVESTIGATION OF IN-PLANE BIAXIAL LOW CYCLE
FATIGUED AUSTENITIC STAINLESS STEEL AISI 321.
II. NEUTRON DIFFRACTION STRESS ANALYSIS
AT THE IBR-2 PULSED NUCLEAR REACTOR

¹Fraunhofer Institute for Non-Destructive Testing, Dresden branch, Germany

²Division of Material Science, Foundation Institute for Materials Science,
Bremen, Germany

³Department of Engineering Science, University of Oxford, UK

Таран Ю. В. и др.

E18-2007-111

Исследование аустенитной нержавеющей стали AISI 321, подвергнутой плоскостному двухосному низкочастотному усталостному циклированию. II. Анализ механических напряжений методом нейтронной дифракции на импульсном ядерном реакторе ИБР-2

Крестообразный образец из аустенитной нержавеющей стали AISI 321, подвергнутый низкочастотному планарному двухосному усталостному циклированию, был исследован на времяпролетном нейтронном фурье-стресс-дифрактометре. Постоянные решеток и объемные доли аустенитной матрицы и мартенситных включений, образованных во время циклирования, измерены вдоль двух взаимно-перпендикулярных планарных осей образца с использованием нейтронного сканера. Компоненты тензора полных остаточных напряжений обеих фаз вычислены из условия равновесия фаз. Разделение остаточных напряжений на макро- и микроскопическую компоненты выполнено с использованием правила смеси фаз. Измерение упругих откликов фаз сделано на одноосной нагрузочной машине. Обнаружено сильное различие между фазовыми упругими модулями.

Работа выполнена в Лаборатории нейтронной физики им. И. М. Франка ОИЯИ.

Сообщение Объединенного института ядерных исследований. Дубна, 2007

Taran Yu. V. et al.

E18-2007-111

Investigation of In-Plane Biaxial Low Cycle Fatigued Austenitic Stainless Steel AISI 321. II. Neutron Diffraction Stress Analysis at the IBR-2 Pulsed Nuclear Reactor

The in-plane biaxial low cycle fatigued sample of the cruciform geometry from austenitic stainless steel AISI 321 was investigated on the time-of-flight neutron Fourier stress-diffractometer. The lattice parameters in the austenite matrix and the martensite inclusions created during the fatigue cycling as well as the martensite volume fraction were measured along two mutually perpendicular planar axes of the sample of the cruciform geometry by using the strain neutron scanner. The phase total residual strain components were calculated using the stress equilibrium relations. The separation of the residual stresses into macro- and microstresses was performed using the mixture rule. The measurements of the applied load-phase elastic strain responses were carried out on a uniaxial load machine. The strong difference between the phase elastic moduli was found out.

The investigation has been performed at the Frank Laboratory of Neutron Physics, JINR.

Communication of the Joint Institute for Nuclear Research. Dubna, 2007

CONTENTS

Introduction	2
1. Experiment Layout	2
2. Spectra Processing and Detector Calibration	4
3. Results of Strain Scanning Spectra Processing	4
4. Phase a_0 -Problem	5
5. Strain/Stress Calculations	9
6. <i>In-situ</i> Uniaxial Stress Rig Measurements	16
Conclusion	18
Acknowledgements	19
References	19

INTRODUCTION

The cruciform geometry sample of Krest-2 from a low carbon Ti-alloyed metastable austenitic stainless steel of the Russian grade GOST 12X18H10T (which is an analogue of the US grade AISI 321 H) was subjected to the in-plane biaxial tension–compression fatigue cycling up to 407 cycles with the frequency of 0.5 Hz at the applied force of 17 kN on the Instron planar biaxial loading machine at Foundation Institute for Materials Science (Bremen) (see details in [1]). The neutron diffraction measurements with the Krest-2 sample were carried out on the FSD stress-diffractometer at the IBR-2 pulsed nuclear reactor (Dubna) in November–December 2006.

1. EXPERIMENT LAYOUT

To measure a radial distribution of the residual stresses in the sample of Krest-2 (Fig. 1) it was installed on the Huber strain scanner at the FSD stress-diffractometer. Two detectors at the scattering angles of $\pm 90^\circ$ (Fig. 2) were used for simultaneous measurements of one of two planar and transverse components of the lattice parameter, respectively. The both detectors consist of some geometry focused ZnS-sections. The spectra from the sections of each detector were focused

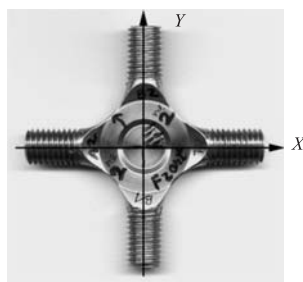


Fig. 1. Sample of Krest-2 with the coordinate system (x, y)

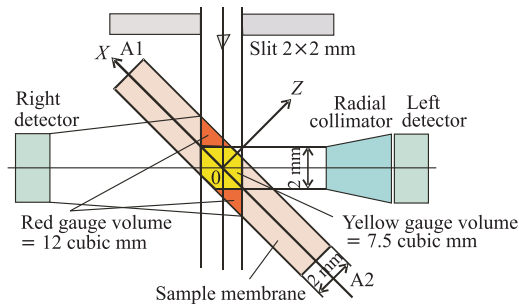


Fig. 2. Layout of the Krest-2 sample membrane with the coordinate system (x, y, z) ; the y -axis is vertical

electronically. The left detector was equipped with the multislit focused radial collimator of 2 mm space resolution. As a thickness of the sample centre part — the 2 mm membrane — was small, the both detectors measured the corresponding lattice parameters averaged on the membrane thickness.

At the beginning of the experiment, the Krest-2 was installed with the horizontal orientation of the A1–A2 cycling direction (x -axis in Fig. 1) and the vertical orientation of the B1–B2 cycling direction (y -axis in Fig. 1). In this case, the layout of the strain scanning is shown in Fig. 2. The right and left detectors measured the lattice parameters along the x -axis (the x -component) and the z -axis (the z -component), respectively. To measure the lattice parameter along the y -axis (the y -component) the sample was rotated through 90° about the z -axis, so the A1–A2 cycling direction was vertical and the B1–B2 cycling direction was horizontal. In this case, the right and left detectors measured the lattice parameters along the y -axis (the y -component) and anew along the z -axis (the z -component), respectively. Altogether, the four strain scans were performed along the x - and y -axes to measure the planar x - and y -components of the residual stress tensor in the austenite and martensite phases. The step of the scan along the x - and y -axes was equal to be of 1.5 mm within the sample membrane of the 15 mm diameter. Thus, five points were measured on the membrane and one point on the leg at $r = 12$ mm for each scan direction.

To measure the mechanical characterization (the applied load-phase elastic strain responses) the sample of Krest-2 was installed inside the TIRA portable electromechanical uniaxial load testing machine placed on the Huber strain scanner (Fig. 3). The x -axis of the sample (Fig. 1) was directed along the horizontal load axis that coincided with the scattering vector of the left detector. The y -axis

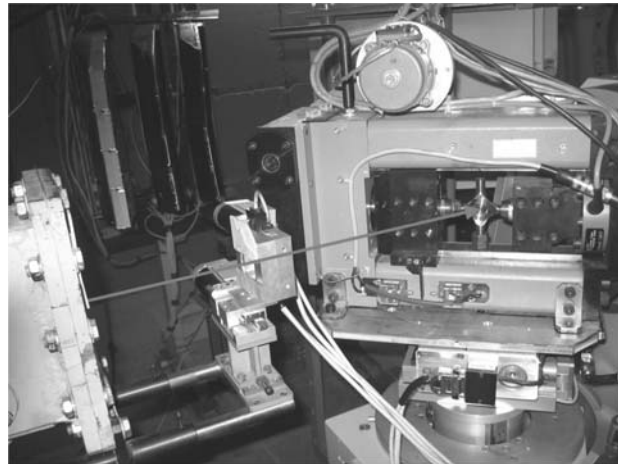


Fig. 3. Sample of Krest-2 inside the TIRA uniaxial load machine in the neutron beam

of the sample was vertical. The radial collimator was removed to increase the scattered beam intensity. Only axial components of the phase lattice parameters were measured during the *in-situ* uniaxial stress rig experiment.

2. SPECTRA PROCESSING AND DETECTOR CALIBRATION

The diffraction spectra were processed by the Rietveld refinement method (two spectra examples are presented in Figs. 4 and 5 for a Ge-sample and the Krest-2 sample, respectively).

All sections of both detectors were calibrated by using the stress-free Ge-powder sample. The Ge-lattice parameter $a = 5.6575 \text{ \AA}$ was taken from «The Powder Diffraction File».

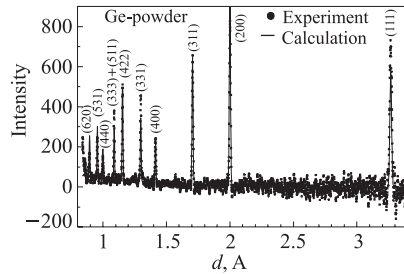


Fig. 4. Diffraction spectrum of Ge-powder from the right detector processed by the Rietveld refinement method

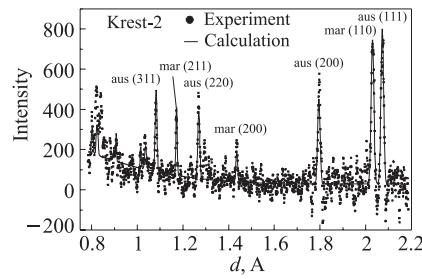


Fig. 5. Diffraction spectrum of the Krest-2 sample from the right detector processed by the Rietveld refinement method

3. RESULTS OF STRAIN SCANNING SPECTRA PROCESSING

In Fig. 6 (*a*, *b*), the results of the planar strain scanning measurements with the right detector are presented as a radial distribution of the (*x*, *y*)-components of the lattice parameters corresponding to the A1–A2 and B1–B2 cycling directions, respectively, for the austenite and martensite phases. The planar data about the austenite and martensite volume fractions are shown in Fig. 7 (*a*, *b*).

The transverse measurements (*z*-axis in Fig. 2) were carried out with the left detector equipped with only ZnS-section and the radial collimator. In this case, the accuracy of data was greatly worse due to strong decreasing of intensity. As we were first of all interested in results of planar measurements, and also taking into account unreliability of results of transverse measurements, we have refused their consideration.

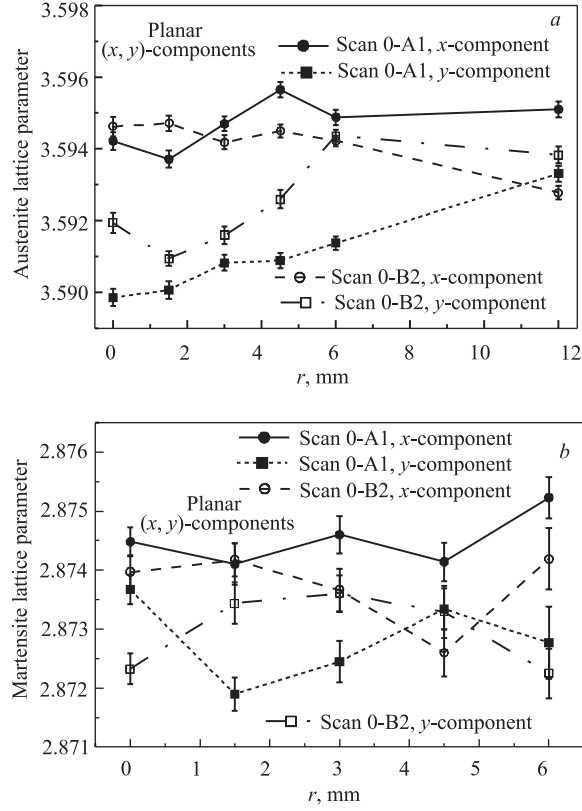


Fig. 6. Radial dependence of the planar components of the phase lattice parameters: a — austenite phase; b — martensite phase

4. PHASE a_0 -PROBLEM

As the austenite matrix is appreciably transformed during the fatigue cycling, and the martensite phase is created in the same process, we could not in principle have the stress-free reference samples of these phases to estimate the residual strains and then the corresponding stresses. Actually, in our disposal there was only an opportunity to make such estimations using results of the austenite lattice parameter measurements on the sample legs, where the plastic deformation is not reached (see Fig. 6 in [1]), and the stress equilibrium approach reviewed in [2] to get martensite a_0 -lattice parameter. In this case, we distinctly understand approximateness of the used approach due to possible inadequacy of the austenite matrix properties in the membrane and the legs, respectively.

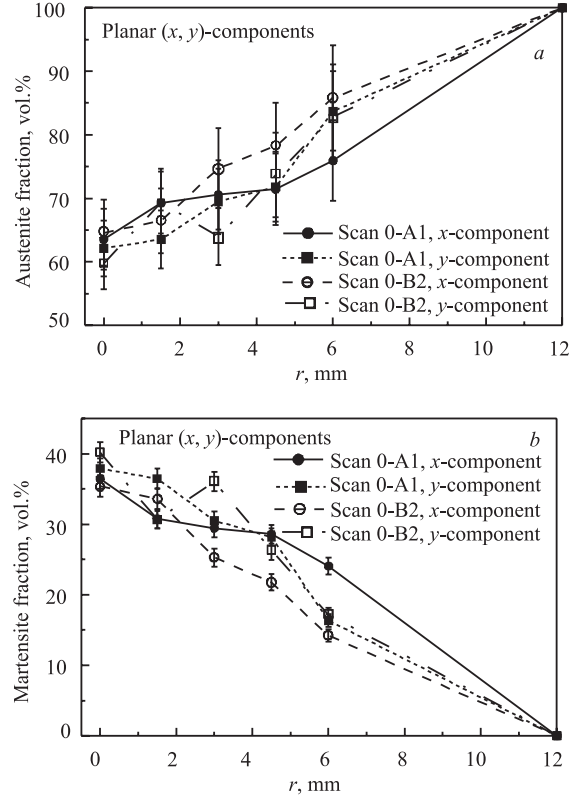


Fig. 7. Radial dependence of the planar components of the phase volume fractions: a — austenite phase; b — martensite phase

Austenite Matrix. As seen in Table 1, the results of the four scans measurements of the planar austenite lattice parameters on the sample legs have almost coincided within triple experimental error that gives the basis to calculate the austenite a_0 -value by their simple averaging equaled to $3.59375(50)$ Å.

Table 1. Legs austenite lattice parameters

Axis	x -component [Å]	y -component [Å]
x (0-A1 direction)	3.59563(22)	3.59489(22)
y (0-B2 direction)	3.59410(20)	3.59610(24)

Martensite Inclusions. To estimate the martensite a_0 -value we have used the approach described in [2]. The phase total residual stress is the sum of the

macrostress and the phase microstress:

$$\langle {}^t\sigma_j^p \rangle = {}^M\sigma_j + \langle {}^\mu\sigma_j^p \rangle, \quad (1)$$

where the carets indicate that the stresses are averaged over the gauge volume (hereinafter, the carets will be omitted for short); the superscripts M and μ denote the macrostress, that is the same in each phase, and the microstress in the p -phase, respectively; the superscript p is equal to a for austenite and m for martensite, respectively; the subscript j indicates the stress component in a sampled point. Each macrostress component must average to zero over the volume of a free body:

$${}^M\bar{\sigma}_j = \frac{1}{V} \int_V {}^M\sigma_j dV = 0, \quad (2)$$

and each phase microstress component must sum to zero when weighted by their volume fraction:

$${}^\mu\sigma_j^a f^a + {}^\mu\sigma_j^m f^m = 0, \quad (3)$$

where f^a and f^m represent the volume fraction of austenite and martensite, respectively ($f^a + f^m = 1$ by definition). Using Eqs.(1)–(3) the macrostress component and the phase microstress components may be determined:

$${}^M\sigma_j = {}^t\sigma_j^a f^a + {}^t\sigma_j^m f^m, \quad (4)$$

$${}^\mu\sigma_j^a = f^m ({}^t\sigma_j^a - {}^t\sigma_j^m), \quad (5)$$

$${}^\mu\sigma_j^m = -f^a ({}^t\sigma_j^a - {}^t\sigma_j^m). \quad (6)$$

Substituting Eq. (4) into Eq. (2) and taking into account that the measurements were made in n -allocated points along i -axis (x or y) of the strain scanning, the integral in Eq. (2) is transformed to a sum:

$$\sum_{k=1}^n [{}^t\sigma_{i,j}^a(x_{i,k}) f_{i,j}^a(x_{i,k}) + {}^t\sigma_{i,j}^m(x_{i,k}) f_{i,j}^m(x_{i,k})] = 0, \quad (7)$$

where the coordinate $x_{i,k}$ corresponds to k -sampled point on i -axis.

The phase total stresses in the sample membrane are planar by definition. In this case, the triaxial Hooke's law may be transformed to the biaxial presentation (the phase index is omitted):

$${}^t\sigma_x = \frac{E}{1+\nu} \left[\varepsilon_x + \frac{\nu}{1-2\nu} (\varepsilon_x + \varepsilon_y + \varepsilon_z) \right], \quad (8)$$

$${}^t\sigma_y = \frac{E}{1+\nu} \left[\varepsilon_y + \frac{\nu}{1-2\nu} (\varepsilon_x + \varepsilon_y + \varepsilon_z) \right], \quad (9)$$

$${}^t\sigma_z = \frac{E}{1+\nu} \left[\varepsilon_z + \frac{\nu}{1-2\nu} (\varepsilon_x + \varepsilon_y + \varepsilon_z) \right] = 0. \quad (10)$$

After simple transformations we shall have

$${}^t\sigma_{i,x} = \frac{E}{1-\nu^2} (\varepsilon_{i,x} + \nu\varepsilon_{i,y}), \quad (11)$$

$${}^t\sigma_{i,y} = \frac{E}{1-\nu^2} (\nu\varepsilon_{i,x} + \varepsilon_{i,y}), \quad (12)$$

where E is the Young modulus, ν is the Poisson ratio, $\varepsilon_{i,j}$ is the phase strain in the coordinate $x_{i,k}$:

$$\varepsilon_{i,j} = \frac{a_{i,j}(x_{i,k}) - a_0}{a_0}, \quad (13)$$

where $a_{i,j}$ is the phase lattice parameter in the same point, a_0 is the stress-free phase lattice parameter. Inserting Eq. (13) into Eqs. (11) and (12) we shall obtain

$${}^t\sigma_{i,x} = \frac{E}{1-\nu^2} \left[\frac{a_{i,x}(x_{i,k}) + \nu a_{i,y}(x_{i,k})}{a_0} - (1+\nu) \right], \quad (14)$$

$${}^t\sigma_{i,y} = \frac{E}{1-\nu^2} \left[\frac{\nu a_{i,x}(x_{i,k}) + a_{i,y}(x_{i,k})}{a_0} - (1+\nu) \right]. \quad (15)$$

Assuming missing of the elastic mismatch between the phases, their elastic constants can be fixed identical. Entering the following designations:

$$\bar{f}_i^p(x_{i,k}) = 0.5[f_{i,x}^p(x_{i,k}) + f_{i,y}^p(x_{i,k})], \quad (16)$$

$$\Sigma f_i^p = \sum_{k=1}^n \bar{f}_i^p(x_{i,k}), \quad (17)$$

$$\bar{a}_{i,X}^p(x_{i,k}) = a_{i,x}^p(x_{i,k}) + \nu a_{i,y}^p(x_{i,k}), \quad (18)$$

$$\bar{a}_{i,Y}^p(x_{i,k}) = \nu a_{i,x}^p(x_{i,k}) + a_{i,y}^p(x_{i,k}), \quad (19)$$

$$\Sigma a_{i,X}^p = \sum_{k=1}^n \bar{a}_{i,X}^p(x_{i,k}) \cdot \bar{f}_i^p(x_{i,k}), \quad (20)$$

$$\Sigma a_{i,Y}^p = \sum_{k=1}^n \bar{a}_{i,Y}^p(x_{i,k}) \cdot \bar{f}_i^p(x_{i,k}), \quad (21)$$

and substituting Eqs. (14) and (15) into Eq. (7) we shall obtain two possible martensite a_0 -values from two scans along the i -axis:

$$a_{0,i,X}^m = \frac{\Sigma a_{i,X}^m}{(1+\nu)(\Sigma f_i^a + \Sigma f_i^m) - \Sigma a_{i,X}^a/a_0^a}, \quad (22)$$

$$a_{0,i,Y}^m = \frac{\Sigma a_{i,Y}^m}{(1 + \nu)(\Sigma f_i^a + \Sigma f_i^m) - \Sigma a_{i,Y}^a / a_0^a}, \quad (23)$$

where a_0^a is the stress-free austenite lattice parameter. Since the strain scans were twice carried out along both x - and y -axes, the four martensite a_0 -values can be obtained from Eqs. (22) and (23).

The results of calculation of the martensite a_0 -values at $\nu = 0.3$ using the average austenite a_0 -value from Table 1 are presented in Table 2. These a_0 -values are close to each other, which gives the basis to obtain the martensite a_0 -value by their simple averaging.

Table 2. Martensite lattice parameters a_0

Axis	x -component [Å]	y -component [Å]
x (0-A1 direction)	2.87405(17334)	2.86912(17271)
y (0-B2 direction)	2.87400(20125)	2.87136(20087)

The anomalously grand experimental errors of the martensite a_0 -values are consciously specified in columns 2, 3 of the table. The point is that these errors are too great mainly due to the large errors in the determination of the austenite and martensite volume fractions by the Rietveld refinement of the diffraction spectra. But, as we have checked by special calculations, the small redistribution of the phase volume fractions is revealed in a weak change of the martensite lattice parameters comparable to the triple experimental error in their measurements. Therefore, it is quite reasonable to attribute to the martensite a_0 -value the standard error of average of the data in Table 2. Thus, the martensite a_0 -value was found to be equal to 2.87213(118) Å.

5. STRAIN/STRESS CALCULATIONS

Austenite Phase. The planar total residual strain components of austenite in the sample membrane are shown in Fig. 8. The calculation was done by using the austenite a_0 -values from Table 1. The results of the austenite total stresses calculation by using $E = 170$ GPa and $\nu = 0.3$ determined in [1] are shown in Fig. 9.

Martensite Phase. The planar total residual strain components of martensite in the sample membrane are presented in Fig. 10. The calculation was done by using the martensite a_0 -values from Table 2. The results of the martensite total residual stresses calculation by using $E = 170$ GPa and $\nu = 0.3$ are shown in Fig. 11. As seen in Figs. 9 and 11, the compression in the austenite phase is balanced by the tension in the martensite phase.

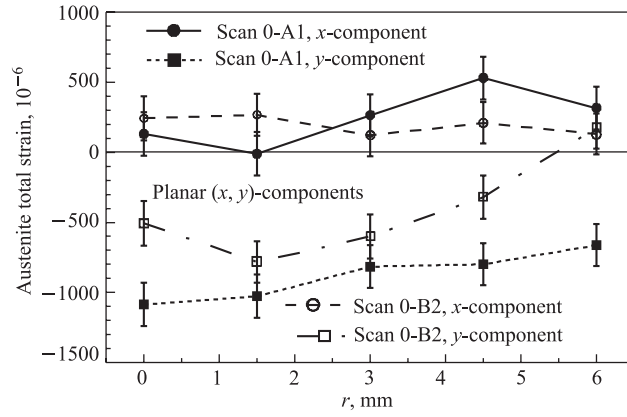


Fig. 8. Radial dependence of the planar total residual strain components of austenite in the sample membrane

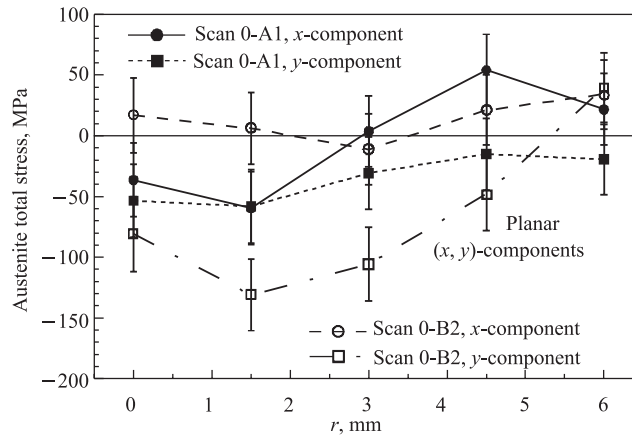


Fig. 9. Radial dependence of the planar total residual stress components of austenite in the sample membrane

Since the total stress measured in any phase is by definition the sum of the macrostress and the microstress in that phase, it is useful to separate the total stress into macro- and microstresses with the purpose to look after the sharing of the microstresses between the austenite and martensite phases along the scan lines with the point-to-point variation of the martensite volume fraction.

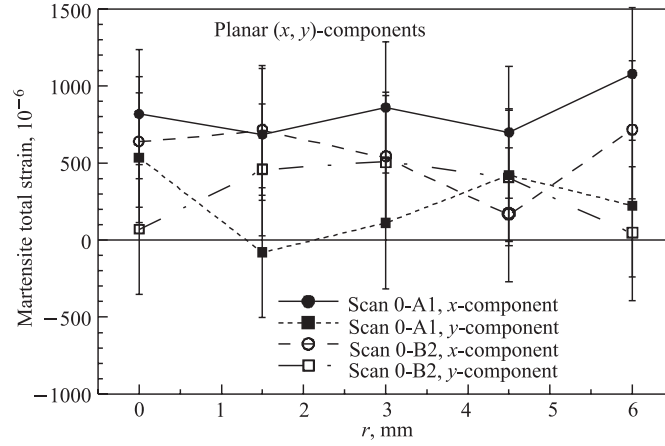


Fig. 10. Radial dependence of the planar total residual strain components of martensite in the sample membrane

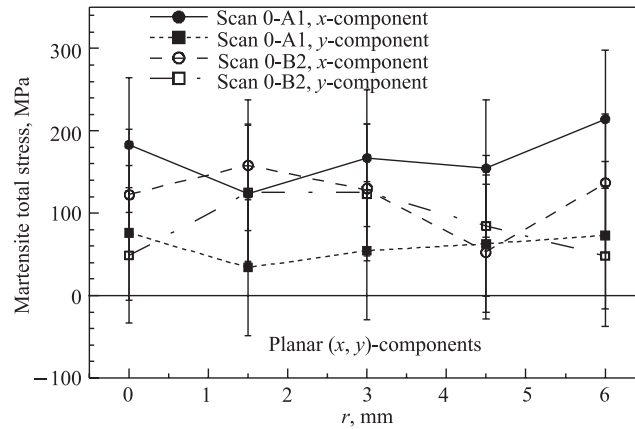


Fig. 11. Radial dependence of the planar total residual stress components of martensite in the sample membrane

Separation of the Phase Total Stresses into Macro- and Microstresses.

According to Eqs. (4)–(6) in two phase materials, it is possible to determine both the macrostresses in the material and the average microstresses present in each phase [2]. The results of such a separation of the phase total residual stresses (see Figs. 9 and 11) are shown in Figs. 12–13.

Since the sample membrane was irradiated through its thickness by the neutron beam, only the planar residual macrostress components were expected dif-

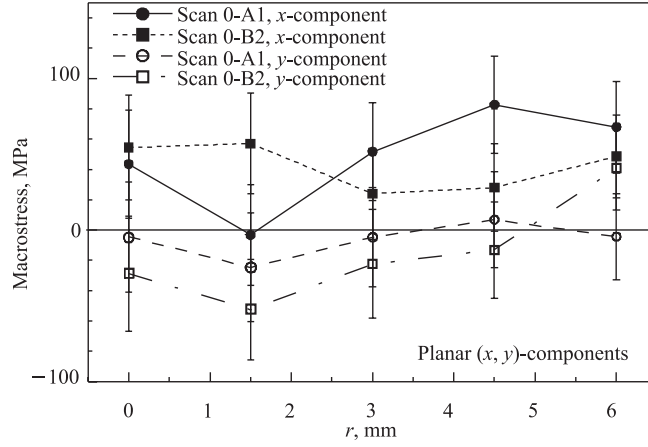


Fig. 12. Radial dependence of the planar macrostress components in the sample membrane

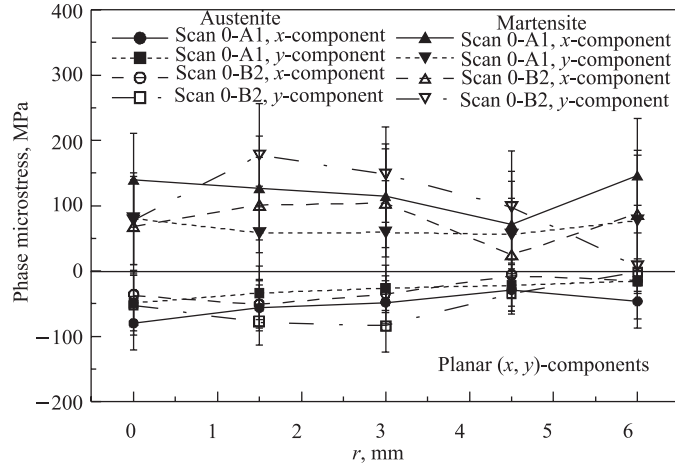


Fig. 13. Radial dependence of the planar phase microstress components in the sample membrane

ferent from zero (Fig. 12). However, their values did not strongly surpass the experimental error. To make a backward check of feasibility of Eq. (2) in our case, the averaged macrostress components ${}^M\bar{\sigma}_j$ along the scan axis were calculated by averaging the experimental data presented in Fig. 12 (Table 3).

Table 3. Averaged macrostresses in the sample membrane

Axis	x -component [MPa]	y -component [MPa]
x (0-A1 direction)	48(32)	-6(32)
y (0-B2 direction)	42(31)	-15(33)

The fact that the averaged residual macrostress was not equal to zero indicates the obvious roughness of the assumptions which were made at determination of the phase stress-free lattice parameters. Especially, it concerns the calculation of the martensite a_0 -value, when integration over the volume of the sample was substituted for simple summation along the scan line. Nevertheless, the result of macrostress separation is satisfactory in view of low precision of the experimental data. The results of separation of the planar phase microstress components (Fig. 15) have shown that the austenite phase is in a compression, while the martensite phase exhibits a balancing tensile stress with the larger value in accordance with the smaller volume fraction. As marked above at discussion of results presented in Figs. 9 and 11, the total residual stresses of the phases were the same signs. This result for the planar phase microstress tensor is unexpected, therefore it requires the special elucidation.

The martensite formation is connected with volume dilation. Since the specific volume of martensite is larger (about 2%) than that of austenite, the martensite phase is generally expected to be in hydrostatic compression, whereas the austenite one is in tension. However, the described experiment demonstrates opposite signs of the microstresses in the phases. A similar phenomenon was observed in the uniaxial low cycle fatigued (LCF) samples from same steel [4]. The effect was interpreted as a superimposition of the phase transformation stresses with the deformation stresses caused by the plastic deformation during LCF. The interplay of these stresses creates the resulting phase residual stress of a non-hydrostatic nature; in this case, the deformation stresses can be overshoot by the phase transformation stresses that were observed in the experiment. The observed rather large tensile microstresses in the martensite could lead to crack initiation.

Separation of the Phase Stress into Hydrostatic and Deviatoric Components. Since the plastic deformation does not occur under hydrostatic (volumetric) pressure, the deviatoric stress tensor often adequately describes the residual stress state with respect to mechanical loading such as fatigue. The phase total stress tensor may be separated into the hydrostatic τ_H^p and deviatoric ${}^t\tau_j^p$ components:

$${}^t\sigma_j^p = {}^t\tau_H^p + {}^t\tau_j^p, \quad (24)$$

where, under definition, $\tau_H^p = (1/3) \text{Tr}({}^t\sigma_i^p)$ and $\text{Tr}({}^t\tau_i^p) = 0$. The phase hydrostatic components τ_H^p were calculated using results of determination of planar total residual stresses of austenite and martensite in the sample membrane (see Figs. 9 and 11) and they are presented in Fig. 14.

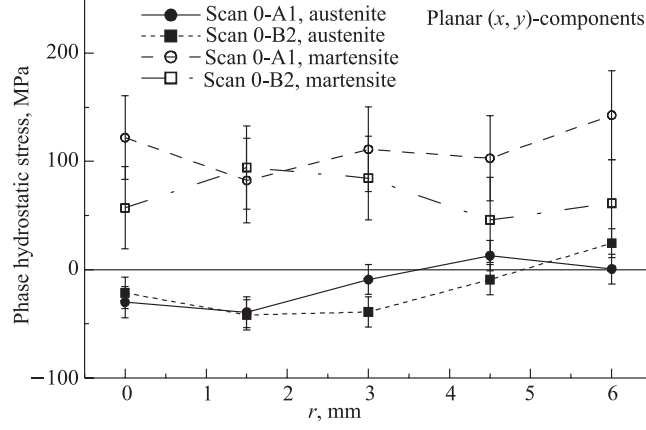


Fig. 14. Radial dependence of the planar phase hydrostatic components in the sample membrane

The result of such a separation has appeared unexpected because the austenite was in hydrostatic compression, whereas the martensite was in tension contrary to the volume dilation representations described above. To clear a situation more detailed mapping of the residual stresses in the sample membrane is necessary.

Since the deviatoric stress tensor is a simple difference between the total and hydrostatic stress tensors we have not represented the result of its calculation. Only note that the character of distribution of the planar deviatoric stresses between the phases was the same as at separation of the microstresses (Fig. 13). The phase transverse deviatoric stresses were equal to the phase hydrostatic stresses with opposite signs.

Biaxial Stresses Difference Approach. The phase total strains/stresses calculated in this section strongly depend on the deviation of a_0 from the true value in each point of the sample. Another approach, e. g., described in [3], may be used to process the biaxial experimental data in the absence of an exact knowledge of a phase a_0 -value, namely, the calculation of the difference between the planar strain/stress components:

$$\delta\varepsilon_{x-y} = \varepsilon_x - \varepsilon_y = \frac{a_x - a_y}{a_0}, \quad (25)$$

$$\delta\sigma_{x-y} = \sigma_x - \sigma_y = \frac{E \cdot \varepsilon_{x-y}}{1 + \nu}. \quad (26)$$

The difference value has feeble sensibility to small deviations of a_0 from its true value, consequently, it is convenient to use the values of $\delta\varepsilon$ and (or) $\delta\sigma$ to

compare the results of the measurements on the different stress-diffractometers as well as the diffraction results with those of the destructive methods and the finite element calculation.

The calculation results of the phase differences of planar total stresses by Eq. (26) using $E = 170$ GPa and $\nu = 0.3$ are shown in Figs. 15 and 16. The calculation was done using the phase a_0 -values from Tables 1 and 2.

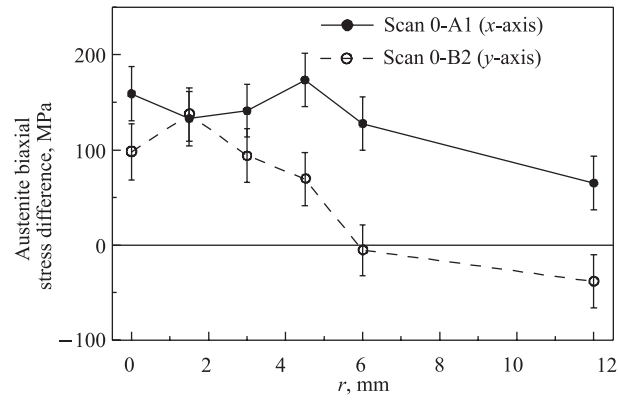


Fig. 15. Radial dependence of the austenite differences of planar total stresses in the sample membrane

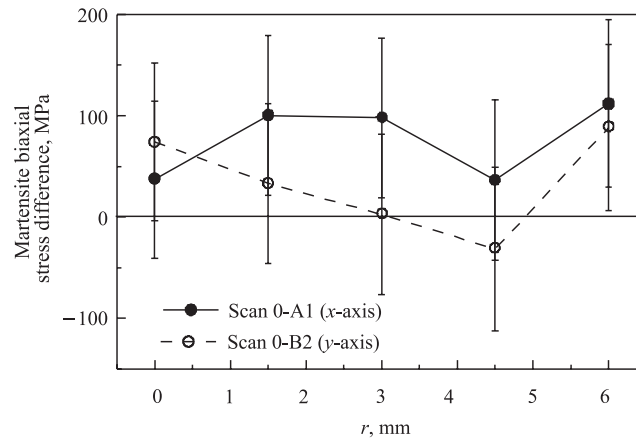


Fig. 16. Radial dependence of the martensite differences of planar total stresses in the sample membrane

6. IN-SITU UNIAXIAL STRESS RIG MEASUREMENTS

The neutron diffraction measurements with the sample of Krest-2 inside the TIRA load machine (Fig. 3) were performed on the FSD stress-diffractometer by using of the left detector. In this case, the load axis was directed along the neutron scattering vector. The measurements were carried out under tension in the elastic region not to deform the original residual stresses map for future more precise investigations. The three repeated runs were made to measure the applied load-elastic strain response in the sample membrane. The dependences of the phase lattice parameters on the applied load for the runs are presented in Fig. 17. The results have appeared poorly reproduced, especially, in the martensite phase. Scattering of the experimental points has much exceeded the measurement errors. Nevertheless, the attempt to obtain the information on the phase elastic constants was undertaken.

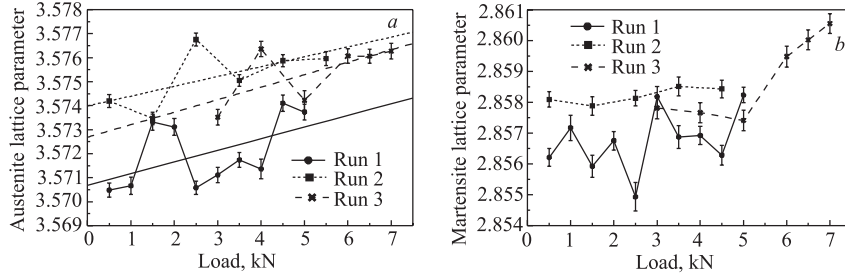


Fig. 17. Phase lattice parameter vs the applied load for the axial direction (tension): *a* — austenite; *b* — martensite

As the slopes of all three curves for the austenite phase (Fig. 17, *a*) are close to each other within the experimental errors the runs were superposed at the zero load. The summary dependence of the austenite lattice parameter on the applied load was linearly fitted in order to calculate the reference lattice parameter a_0 at the zero load and the curve slope B . The fit results were the following: $a_0 = 3.57285(14) \text{ \AA}$, $B = 4.91(35) \cdot 10^{-4}$. The applied load-austenite total elastic strain response calculated using the obtained a_0 -value is presented in Fig. 18.

As it is easy to show, the slope B of the summary dependence may be expressed through the Young modulus E and the effective cross section S_{eff} of the load application on the membrane:

$$B = a_0 / (100ES_{\text{eff}}), \quad (27)$$

where E is in GPa and S_{eff} is in cm^2 . Using $E = 170$ GPa measured during the quasistatic uniaxial testing on the Instron machine, the effective cross section S_{eff} was calculated to be equal to $0.43(3)$ cm^2 compared to the geometrical cross section S_{geo} of the membrane in the sample centre equalled to $0.2 \text{ cm} \times 1.5 \text{ cm} = 0.3 \text{ cm}^2$.

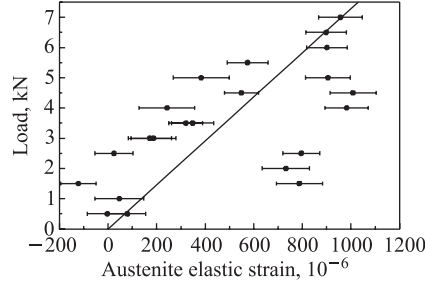


Fig. 18. Applied load-austenite elastic strain response for the axial direction under tension

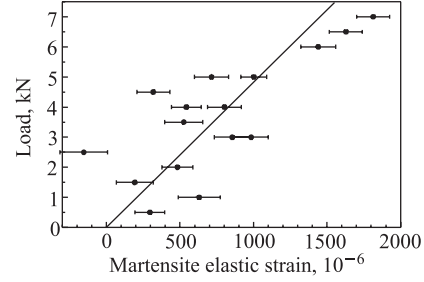


Fig. 19. Applied load-martensite elastic strain response for the axial direction under tension

As the slopes of all three curves for the martensite phase (Fig. 17, *b*) are different from each other, the superposition of the runs by the way used for the austenite phase was impossible. However, if to discard run No. 2 and to sum only runs Nos. 1 and 3, the results of linear fit of the summary curve have appeared the following: $a_0 = 2.85537(19) \text{ \AA}$, $B = 5.91(44) \cdot 10^{-4}$. The applied load-martensite total elastic strain response calculated using the obtained a_0 -value is presented in Fig. 19. Using the effective cross section S_{eff} obtained for the austenite phase, the martensite Young modulus was calculated to be equal to $112(17)$ GPa, which strongly differs from the austenite modulus. Seemingly, this result indicates the large elastic mismatch between the phases, however, it is necessary to consider it with great care due to large scattering of the experimental points and bad reproducibility of the response measurements. Note that the moderate elastic mismatch between the austenite and martensite phases was first observed in the uniaxial high cycle fatigued samples of same steel [5]. However, the uniaxial low cycle fatigued samples have not got any elastic mismatch between the phases [6]. In the case, more precise and reliable measurements of the applied load-phase elastic strain responses in the in-plane biaxial low cycle fatigued sample of the cruciform geometry are necessary. Reliable gripping of the sample in the testing machine and precise control of the location of thin sample membrane in the neutron beam are crucial here.

CONCLUSION

The in-plane biaxial low cycle fatigued sample of the cruciform geometry from a low carbon Ti-alloyed metastable austenitic stainless steel of the Russian grade GOST 12X18H10T (an analogue of the US grade AISI 321 H) was investigated on the FSD Fourier neutron stress-diffractometer at the IBR-2 pulsed nuclear reactor (Dubna).

The lattice parameters in the austenite matrix and the martensite inclusions created during the fatigue cycling as well as the martensite volume fraction were measured along two mutually perpendicular planar axes of the sample of the cruciform geometry. The martensite fraction is changed from 38% in the sample centre to 18% at circumference.

The phase total residual strain/stress components were calculated from the experimental data by using the phase stress-free lattice parameters a_0 . The austenite a_0 -value was measured in two out of four legs of the cruciform sample, where the plastic deformation during the fatigue cycling was small and could not create the appreciable martensite volume fraction. The martensite a_0 -value was calculated from the experimental data using the austenite a_0 -value and the stress equilibrium relations.

The calculation of the total residual stresses have shown that the austenite phase is in a compression, while the martensite phase exhibits a balancing tensile stress with the larger value in accordance with the smaller volume fraction. The separation of the phase total stresses into the residual macro- and microstresses was performed using the mixture rule. The macrostresses were small and did not strongly surpass the experimental error. Contrary to expectations, the calculation of the microstresses has shown that the compression in the austenite is balanced by the tension in the martensite. A similar phenomenon was observed in the uniaxial LCF samples from the same steel [4] which was interpreted as a superimposition of the phase transformation stresses with the deformation stresses caused by the plastic deformation during fatigue cycling.

The phase hydrostatic components separated from the phase total stresses were of the same signs as in the total stresses contrary to volume dilation representations. Apparently, the reason is in shortage of the experimental data as the strain scanning was performed along only two axes; in this case, a segment between the axes was not covered by the measurements. Note the too rough assumptions made at calculation of the phase total stresses. More detailed mapping of the residual stresses into the sample membrane would be performed to clear a situation.

The measurements of the applied load-phase elastic strain responses in the elastic region were carried out in the membrane centre of the cruciform sample along one of two cycling axes using the TIRA uniaxial load machine. The effective cross section of the load application on the sample membrane was

determined from the austenite response with the help of the austenite elastic modulus measured in [1]. The martensite elastic modulus was calculated from the corresponding strain response using the effective cross section determined from the austenite response. The martensite modulus strongly differs from the austenite one. Seemingly, this result indicates the large elastic mismatch between the phases, however, it is necessary to consider it with great care in a kind by bad reproducibility of the responses measurements. Note that the moderate elastic mismatch between the austenite and martensite phases was previously observed in the uniaxial high cycle fatigued samples of same steel [5], but it has missed in the uniaxial low cycle fatigued samples [6]. The more precise and reliable measurements of the applied load-phase elastic strain responses of the in-plane biaxial low cycle fatigued sample of the cruciform geometry would be carried out to solve the problem.

Acknowledgements. The authors wish to thank A.N. Kuznetsov (FLNP JINR), Ch. Stoerberl (FIMS) and P. Rathjen (FIMS) for large help in preparation and testing of the cruciform samples for the neutron diffraction experiments. The special gratitude is to W. J. J. Vorster (UO) for the calculations of the stresses in a sample of the cruciform geometry by the finite element method. Thanks are also to I. V. Papushkin (FLNP JINR) who has assisted in preparation and carrying-out of the neutron diffraction measurements on the FSD stress-diffractometer.

REFERENCES

1. *Taran Yu. V., Balagurov A. M., Kuznetsov A. N. et al.* JINR Commun. E18-2007-110. Dubna, 2007.
2. *Winholtz R. A.* Separation of Microstresses and Macro stresses // Measurements of Residual and Applied Stress Using Neutron Diffraction / Eds. M. T. Hutchings, A. D. Krawitz. Dordrech; Kluwer Academic Publishers, 1992. P. 131–145.
3. *Taran Yu. V., Schreiber J., Mikula P. et al.* // Proc. of the 4th European Conf. of Residual Stresses, Cluny, France, June 1996. P. 87–95.
4. *Taran Yu. V., Daymond M. R., Schreiber J.* // Physica B. 2004. V. 350. P. 98–101.
5. *Taran Yu. V., Daymond M. R., Schreiber J.* // J. Appl. Phys. A. 2002. V. 74. P. S1385–S1387.
6. *Taran Yu. V., Daymond M. R., Eifler D., Schreiber J.* // Ibid. P. S1391–S1393.

Received on July 18, 2007.

Редактор *В. В. Булатова*

Подписано в печать 11.01.2008.

Формат 60 × 90/16. Бумага офсетная. Печать офсетная.

Усл. печ. л. 1,37. Уч.-изд. л. 1,91. Тираж 280 экз. Заказ № 56018.

Издательский отдел Объединенного института ядерных исследований
141980, г. Дубна, Московская обл., ул. Жолио-Кюри, 6.

E-mail: publish@jinr.ru

www.jinr.ru/publish/